Structural characteristics and residual stresses in oxide films produced on Ti by pulsed unipolar plasma electrolytic oxidation

Raja H.U. Khan, Aleksey Yerokhin, A Matthews

Structural characteristics and residual stresses in oxide films produced on Ti by pulsed unipolar plasma electrolytic oxidation

Journal:	*Philosophical Magazine & Philosophical Magazine Letters*
Manuscript ID:	TPHM-07-Nov-0322.R1
Journal Selection:	Philosophical Magazine
Date Submitted by the Author:	31-Jan-2008
Complete List of Authors:	Khan, Raja; University of Sheffield, Engineering Materials Yerokhin, Aleksey; University of Sheffield, Engineering Materials Matthews, A; University of Sheffield, Engineering Materials
Keywords:	oxide films, titanium
Keywords (user supplied):	Plasma electrolytic oxidation, residual stresses, pulsed unipolar current

Structural characteristics and residual stresses in oxide films produced on Ti by pulsed unipolar plasma electrolytic oxidation

R.H.U. Khan, A.L. Yerokhin[1] and A. Matthews

Department of Engineering Materials, University of Sheffield, Mappin Street, Sheffield S1 3JD, UK

Abstract

Oxide films, 7 to 10 μm thick, were produced on commercially pure titanium by plasma electrolytic oxidation in a sodium orthophosphate electrolyte using a pulsed unipolar current with frequency (f) and duty cycle (δ) varied within f = 0.1 to 10 kHz and δ = 0.8 to 0.2 respectively. The coatings comprised a mixture of an amorphous phase with nanocrystalline anatase and rutile phases wherein the relative content of rutile varied from 17 to 25 wt%. Incorporation of phosphorus from the electrolyte into the coating in the form of PO_2^-, PO_3^{2-} and PO_4^{3-}, as demonstrated by EDX and FT-IR analyses, seems to contributed the formation of the amorphous phase. Residual stresses associated with the crystalline coating phase constituents were evaluated using the X-ray diffraction $\sin^2\psi$ method. It was found that, depending on the treatment parameters, internal direct and shear stresses in anatase ranged from -205 (±17) MPa to -431 (±27) MPa and from -98 (±6) MPa to -145 (±10) MPa respectively, whereas the rutile structure is comparatively stress free.

Keywords: Plasma electrolytic oxidation; pulsed unipolar current; nanocrystalline; anatase; rutile; residual stresses; X-ray diffraction

[1] - Corresponding author. Department of Engineering Materials, University of Sheffield, Sir Robert Hadfield Building, Mappin Street, Sheffield, S1 3JD, United Kingdom. Tel: +44 1142225510; FAX: +44 1142225943; E-mail: A.Yerokhin@sheffield.ac.uk

1. Introduction

Plasma electrolytic oxidation (PEO) has attracted considerable attention due to its major advantages, such as environmental friendliness, capability of fabricating oxide films with controlled morphology and composition, good adhesion to the metal substrate, and wear- and corrosion- resistance [1]. These advantages allow PEO to be considered as an alternative to conventional acid-based anodising processes for titanium and its alloys [2-4].

During PEO, the oxide film formation is influenced by plasma microdischarge events which provide multiple heating-cooling cycles to the surface, affecting the film structure, phase composition and stress state. The microdischarge characteristics can be controlled by the current mode applied, e.g. through variation in the shape of the current waveform, its amplitude, frequency and duty cycle. Among the three main current modes used in PEO, i.e. DC, AC and pulsed current regimes, the latter offers maximum flexibility in process control. This could provide a valuable means to control important characteristics, especially internal stresses in PEO coatings, thereby tailoring their performance, as it is generally accepted that such stresses influence directly or indirectly almost all properties of coated materials, including mechanical (e.g. hardness, adhesion, wear- and corrosion- resistance, fatigue crack propagation), barrier and magnetic ones. For example, in most situations where mechanical performance of the coating-substrate system is paramount, either minimisation of internal stresses or generation of a moderately compressive stress state in the coating is considered to be beneficial [5, 6].

Despite the importance of internal stress for the physical and mechanical properties in titania coatings, only a few studies have addressed this issue in general [7-13] and even fewer looked at

the PEO titania coatings as well [14, 15]. However, no systematic studies of the effects of pulsed current on the internal stress in PEO coating on titanium have been reported.

Earlier, it was demonstrated that for the pulsed current PEO of aluminium in alkaline solutions the coating stress state varies significantly along with its structure and phase composition, depending on the frequency (f) and duty cycle (δ) of the current pulses applied [16]. Investigation of associated effects in PEO coatings on other materials, in particular Ti, is therefore of great interest. In this work, the influence of pulsed unipolar current is studied on the residual stresses in PEO coatings produced on commercially pure titanium (cp-Ti) at different f and δ values in a sodium orthophosphate electrolyte and the internal stresses have been evaluated using the X-ray diffraction $Sin^2 \psi$ technique.

2. Experimental Procedures

2.1 Sample preparation

Rectangular cp-Ti coupons with dimensions 25 mm × 23 mm × 0.75 mm were used as substrates. Prior to PEO treatment, these were mechanically polished to achieve a surface finish of Ra ≈ 0.1 µm, then ultrasonically cleaned in ethanol and dried.

2.2 PEO treatment

PEO coatings were formed with an electrolytic plasma unit consisted of a DC power supply, a pulsing unit and a stainless steel container equipped with stirring and cooling systems. The sample and container walls were used as the anode and the cathode respectively. An electrolyte prepared with a solution of 10 g/l $Na_3PO_4 \times 12H_2O$ in distilled water was cooled to remain below 25°C throughout the treatment.

The reference coating was produced using direct current (DC); for other coatings, a pulsed unipolar current mode was applied, with f and δ values ranging from 0.1 to 10 kHz and from 0.8 to 0.2 respectively. All coatings were formed for 10 min at a constant mean average current density i = 10 A/dm^2 (Fig 1).

2.3 Coating characterisation

2.3.1 Thickness measurements

Coating thicknesses were measured using an Elcometer 355 modular thickness gauge system equipped with standard No 4 Anodisers probe with an accuracy of about ±1 μm. Ten random measurements were taken from a coated surface followed by statistical analysis to determine the mean thickness value and its scatter.

2.3.2 Phase analysis and surface morphology

To evaluate coating phase composition, X-ray diffraction (XRD) patterns were obtained using a Siemens D5000 X-ray diffractometer (Cu Kα radiation, λ=15.4059 nm) operated at 30 mA tube current and 40 kV accelerating voltage. The scans (Fig. 2) were carried out using a θ/2θ geometry in the 2θ range from 20° to 90° with 0.02° step size. The XRD patterns were also used to estimate the relative weight fraction of rutile (x) and the crystallite sizes of the coating phase constituents. The former was estimated using the following equation [17, 18]:

$$x = \left(1 + 0.8\frac{I_A}{I_R}\right)^{-1} \qquad (1)$$

where I_A and I_R are the integrated x-ray intensities of the strongest anatase and rutile peaks corresponding to (101) anatase and (110) rutile planes at 2θ = 25.3° and 27.4° respectively. The latter was derived from broadening of the same peaks, using the Scherrer formula [19]:

$$t = \frac{0.9\lambda}{B\cos\theta} \qquad (2)$$

where t is the crystal thickness measured in a direction perpendicular to a particular set of Bragg planes and B is the line width at half maximum height (FWHM).

SEM observations were made using a Camscan electron microscope from the surface of PEO coatings sputter-coated with carbon to minimize surface charging, along with EDX analyses to evaluate coating elemental composition. To evaluate the chemical state of phosphorus in the coatings, Fourier transform infrared (FT-IR) spectra were obtained in the range from 4000 to 400 cm^{-1} at a resolution of 4 cm^{-1} using a Perkin Elmer 200 FT-IR spectrometer (USA) operated in reflection mode.

2.3.3 Nanoindentation

To evaluate mechanical properties of PEO coatings on a sub-micron level, nanoindentation tests were performed using a Hysitron Triboscope instrument equipped with a Scanning Tunnelling Microscope (STM). Normally, 2 to 3 sets of 7×7 measurements, each covering a surface area of approximately 30 μm × 30 μm, were carried out on the coating cross-section. The method of Oliver and Pharr was used for the analysis of the unloading part of the load-displacement curve to determine hardness (H) and Young's modulus (E). Obtained H and E maps were compared to the corresponding STM image to separate the values actually attributed to the coating from those of the substrate. Another refinement was made in regard to the measurements affected by apparent coating defects, e.g. microcracks and large pores. The accumulated coating data were then subjected to a statistical analysis to determine mean average values of Young's moduli corresponding to different phase constituents; these were used for the conversion of strain into residual stresses.

2.3.4 Stress measurement

Residual stresses were measured in the anatase and rutile phases of the coating by the XRD Sin^2 ψ method. Elliptical fitting between the fractional change of the plane spacing (i.e. strain) and Sin^2 ψ was performed to evaluate both direct (i.e. acting normal to the surface of a plane) and shear (i.e. acting parallel to the surface of a plane) stress components. The measurements were carried out for anatase and rutile at 9 ψ angles (from – 36° to + 36°) and 7 ψ angles (from – 18° to + 18°) respectively with 0.01° (2θ) step size and 90 s exposure time. The gravity peak location method [16, 20] with 10% threshold value was employed to calculate (215) anatase (Fig. 3a) and (222) rutile (Fig. 3b) peaks positions at 2θ = 75.032° and 89.557° respectively using Bruker Stress software [21].

3. Results

3.1 Coating thickness

Coating thickness measured for the reference DC sample was 8.8 µm, whereas the thicknesses of the coatings produced under pulsed current conditions varied in the range from 7.1 µm to 9.8 µm. Although this variance lay within the instrumental error, a trend was observed for the thickness to decrease slightly when duty cycle was decreased from δ = 0.8 to δ=0.2.

3.2 Surface morphology

SEM observations reveal a typical PEO coating surface morphology featuring developed porosity and sub-micron grain structure (Fig. 4). For the pulsed unipolar coatings, the surface morphology is similar to that of the reference DC coating; moreover it does not show any considerable variation with the process parameters (f and δ). The open surface porosity ranges from several microns (Fig. 4a) to a sub-micron scale (Fig. 4b). It is formed by large irregular pores that are

often superposed by medium-size (~ 1 μm) pores and characteristic nodular features with fine (~ 50-100 nm) pores. Fused and resolidified masses often appear, especially around large and medium pores, with their smoothened edges resembling volcano tops. This however is much less evident in fine porosity. Occasional surface cracks can be seen at higher magnification (Fig 4b), which is indicative of the stress generation and relaxation processes occurring during coating formation.

3.3 Surface phase analysis

The typical XRD spectrum presented in Fig. 2 indicates that anatase and rutile are the major crystalline phases in the coating. Figure 5 shows that the relative rutile content in the coatings produced using pulsed current varies from 17 to 25 wt%; this is consistent with the reference DC sample (22 wt%). This characteristic is barely affected by the pulse duty cycle while the frequency dependencies appear to have a minimum at f = 1 kHz.

The average crystallite sizes in the coatings produced using pulsed current are evaluated to be 32 and 36 nm for anatase and rutile respectively, which is very close to the corresponding values (31 and 34 nm) obtained for the reference DC coating. These results are in good agreement with previous work done by other research groups [17, 22].

Apart from crystalline phases, evidence of some amorphous components can be traced in the XRD pattern (Fig. 2), in particular within the 2θ range from 20^{o} to 35^{o}. Amorphisation of PEO titania coatings is usually associated with incorporation of phosphorus species from the electrolyte during the oxidation process [23, 24]. Indeed, EDX analysis revealed the presence of some phosphorus in the coatings produced, while qualitative FT-IR results (Fig. 6) showed characteristic reflections at frequency bands/cm^{-1} 1250-1290, 1160-1170 and 840-870 that can be attributed to PO_2^-, PO_3^{2-} and PO_4^{3-} groups respectively [25-27]. Thus the existence of an

amorphous phase in the coatings studied in this work can also be linked to the incorporation of (poly) phosphate compounds.

3.4 Nanoindentation

Fig. 7a shows typical STM image of the coating cross-section, whereas Figs. 7b and 6c represent maps of hardness and Young's modulus corresponding to the central region outlined in Fig. 7a. The global elastic modulus and hardness of the coatings rang from 60 to 220 GPa and from 2 to 12 GPa respectively. Insulated regions of higher hardness and stiffness can be observed in the middle part of the coating, corresponding probably to rutile-enriched sites. The mean average value of Young's modulus for these areas was evaluated to be 180 GPa, whereas for the reminder of the coating it was found to be 110 GPa; these were used for stress evaluation in rutile and anatase respectively. It should be noted that the values of Young's modulus and hardness accepted for rutile and anatase in this work are lower compared with the values reported by other researchers [28]. Fine occluded porosity, amorphous compounds and the nanocrystalline structure of the coatings should be responsible for the decreased values of these properties.

3.5 Residual stresses

3.5.1 Stresses in Anatase

Figure 8 shows the results of residual stress evaluation in the anatase phase. Direct stresses in the reference DC coating are found to be compressive -257±23 MPa and depending on the parameters of pulsed current they are varied from -205MPa to -431MPa (Fig. 8a). The lower values (-205 to -250 MPa) correspond to $\delta = 0.8$, at which direct stresses are barely affected by the pulse frequency. At $\delta < 0.8$, the stresses are always higher than in the reference DC coating and tend to increase with both increased frequency and decreased duty cycle, so that the highest

value (-431±27 MPa) is found at the corner point of the experimental design (δ = 0.2; f = 10 kHz).

Shear stresses in the anatase phase for the reference DC coating are evaluated to be -105±7 MPa. The stress values in the pulsed unipolar coatings lie in the range -98±6 MPa to -145±10 MPa as shown in Fig. 8b. These are normally slightly higher than in the reference DC coating except for the samples treated at δ = 0.8 and 0.6 and f = 1 kHz. Depending on the parameters of pulsed current (f and δ), shear stresses show behaviour that is similar to direct stresses.

3.5.2 Stresses in Rutile

Results of residual stress evaluation in rutile phase are shown in Fig. 9. Direct stresses are found to be compressive -78±3 MPa in the reference DC coating and they are generally slightly higher (-100 to -180 MPa) in the coatings produced using pulsed current (Fig. 9a). The direct stresses do not show much variation with the duty cycle whereas clear minima are observed at f = 1 kHz in all frequency dependencies.

Unlike anatase, the shear stresses estimated in the rutile are positive (Fig. 9b), i.e. (53±3 MPa) and (25±4 MPa to 83±6 MPa) for the coatings produced using DC and the pulsed unipolar current respectively. For the latter coatings, frequency dependencies tend to converge towards the DC value at f = 1 kHz. However the absolute values of shear stresses are rather negligible, bearing in mind the inherent experimental error (±50 MPa) of the method used.

4. Discussion

Several outcomes of the present work related primarily to the coating formation using pulsed unipolar current and associated evolution of their stress state would require a detailed discussion.

4.1 Formation of PEO coatings on cp-Ti under pulsed current conditions

Firstly, it was found that, in contrast with Al [16], thickness and morphology of PEO films produced on Ti do not significantly depend on the parameters of pulsed current, i.e. f and δ. This can be associated with the following two factors: (i) mechanisms of the coating formation and (ii) characteristics of current regimes employed. The growth of PEO coatings on Al in alkaline solutions is known to be affected by electrochemical oxide dissolution which can be suppressed by increased current density [30,31]. A proportional to δ decrease in i at a constant current during pulse ON time employed in [16] has predictably resulted in thinner and more porous coatings with decreased pulse duty cycles. In contrast, PEO of Ti in phosphate electrolytes is not affected by electrochemical oxide dissolution [33] and the current mode employed in the present study allowed maintaining constant i throughout the process (Fig. 1); this led to the formation of coatings that are similar in thickness and morphology regardless of f and δ. This implies that the electrolyte concentration and the mean average current density (rather than the instantaneous pulse current) are likely to be important factors affecting coating formation during PEO of Ti in phosphate solutions.

Secondly, distinctive features of titania coatings produced in this work were found to include a deconvoluted surface morphology formed by a superposition of diverse porosity and a nano grain crystalline structure. These can be explained by plasma discharge effects on the forming oxide film. Origination of large irregular pores is likely to be triggered by film blistering and rupture sometimes observed prior to discharge onset on Ti [34]. Apparently this is linked to a relaxation of internal stresses that could be caused by several reasons, e.g. high Pilling-Bedworth ratio (PBR) for Ti, coalescence of molecular oxygen in the film due to relatively high electronic conductivity of titania and crystallisation of originally amorphous oxide film. Whatever the reason, cracks formed provide sites of increased conductivity favourable for occurrence of

microdischarge events. Corresponding flashes of high temperature and pressure lead to melting and re-solidification of adjacent coating and substrate regions. Rapid temperature increases reduce gas solubility in the melt; this results in fine porosity and nodular features being quenched on the surface as observed in Fig 4. Rapid solidification also promotes formation of nanocrystalline phases as well as coating amorphisation. This is confirmed by XRD studies (Fig. 2) and evaluations using equation (2). The amorphisation is enhanced by incorporation of phosphate species from the electrolyte (Figs. 4c and 6), which occurs through both anionic adsorption and plasma-assisted chemical interactions within discharge regions. The crystalline structure of PEO coatings comprises a matrix of metastable anatase with thermodynamically stable rutile inclusions. In all coatings, relative rutile content (17-25 wt%, Fig. 5) is insufficient to form a skeleton; this is consistent with nanoindentation results (Fig. 7). For PEO of Al, Guangliang, et al [35] have found that there is a threshold value of current density (~10 A dm^{-2}) beyond which the content of α-alumina in the coating increases sharply. It would be reasonable to assume the existence of similar threshold for PEO-titania coatings too. The fact that the parameters of pulsed current used in this work do not affect the rutile content significantly indicates this threshold value of current density has not been reached. This is probably due to the stabilising effect of phosphate species on anatase [36].

4.2 Factors affecting internal stresses in PEO coatings on Ti

It appears that, unlike structural characteristics, the coating stress state shows considerable variations with the parameters of pulsed current. Not surprisingly, this is primarily concerned with the anatase matrix, whereas rutile inclusions are relatively relaxed. A rational explanation to the observed behaviour can be found when considering a competition between stress generation and relaxation processes during the coating growth. Taking account of the sign of the resulting

stresses in anatase, Pilling-Bedworth ratio (PBR), electrostriction as well as discharge induced thermal gradients and phase transformations are considered here as stress generation factors. At the same time, crystallisation of amorphous titania, thermal annealing (due to heating by discharge) and crack formation contribute to the stress relaxation.

4.2.1 Stress generation

Pilling-Bedworth stresses. High PBR = 1.73 for Ti is responsible for large stress generation at the coating-substrate interface, in particular during initial anodising stages. The positive PBR value indicates that the oxide film is put under compression proportionally to its thickness. Since the coatings produced here possess similar thicknesses and phase compositions, the contribution of the PBR component to the overall coating stress state is deemed to be similar for all coatings.

Electrostrictive stresses that depend upon the applied potential during the process provide an additional compressive component to the instantaneous stress state during oxide growth [12]. This stress component increases with decreased δ according to the magnitude of voltage pulses, which is consistent with data of Fig. 8.

Thermal stresses can be categorised as: (i) stresses caused by differential thermal expansion between coating and substrate and (ii) stresses caused by temperature gradients occurring within the coating during treatment. In both cases these are governed by thermal expansion coefficients α of corresponding phases. Since $\alpha_{anatase} = 10.2\times10^{-6}\ ^{o}C^{-1} > \alpha_{Ti} = 8.9\times10^{-6}\ ^{o}C^{-1} > \alpha_{rutile} = 7.14\times10^{-6}\ ^{o}C^{-1}$ [29], thermal stresses with respect to the Ti substrate should contribute another compressive component in anatase and a tensile component in rutile. This is consistent with absolute values of stresses observed in corresponding phase constituents (Figs. 8 and 9).

Stresses caused by phase transformation are mainly due to the anatase–to–rutile transition, as anatase has a larger unit cell volume and lower density than rutile (0.136 nm^3, 3.84 g/cm^3 and 0.062 nm^3, 4.26 g/cm^3, respectively) This should relax the anatase matrix and contribute an

additional tensile stress component in rutile due to the decrease in unit cell volume. However, the resulting stress state of rutile is likely to be affected by the absence of a continuous rutile skeleton within the coatings, as evident from nearly negligible values of shear stresses in rutile (Fig. 9b).

4.2.2 Stress relaxation

Stress relaxation caused by crystallisation is mainly due to amorphous titania (formed during the initial stages of the PEO process) crystallisation into the anatase during coating formation. It is worth noting that, apart from thermal stress generation, the discharges is responsible for thermal annealing that occurs in the vicinity and within the local discharge regions. The effect of annealing should become more pronounced with increased duration of current pulses, i.e. at lower frequencies; this indeed is noticeable in Fig. 8a. As discussed, the stresses are also relaxed due to crack formation in the coatings and evidenced during higher magnification SEM studies (Fig. 4b). However this appears to have no systematic effect on the coating stress state.

5. Conclusions

Based on the results obtained it can be concluded that:

1. Oxide films 7 to 10 μm in thicknesses were produced on commercially pure titanium by plasma electrolytic oxidation in a sodium phosphate electrolyte using pulsed unipolar current. Higher coating thickness (i.e. 10 μm) was found at δ=0.8, whereas the value was found lower (i.e. 7 μm) at δ=0.2.

2. The films are mainly composed of anatase and rutile phases, with relative content of rutile being in the range 17–25 wt%. Regardless f and δ, the average crystallite sizes of the anatase and rutile are 32 and 36 nm respectively.

3. Phosphorus is present in the amorphous phase of the coatings in the form of PO_2^-, PO_3^{2-} and or PO_4^{3-} which incorporated from the sodium phosphate electrolyte.

4. Coating thickness, surface morphology, phase composition and residual stress are not greatly affected by the parameters of pulsed unipolar current (f=0.1 to 10 kHz and δ=0.8 to 0.2) used during PEO treatment of titanium.

5. Direct and shear stresses in anatase were found in the ranges from (-205±17 MPa to -431±27 MPa) and (-98±6 MPa to -145±10 MPa) respectively. Direct stress in anatase increase with increased frequency and decreased duty cycle of pulsed current. This is mainly attributed to the effects of electrostriction and thermal annealing by the plasma discharge.

6. Direct and shear stresses in rutile were comparatively low and are found in the range from (-52±9 MPa to -177±11 MPa) and (25±4 MPa to 83±6 MPa) respectively. The absence of shear components indicated that the rutile is unlikely to form a continuous skeleton structure within the coating.

6. Acknowledgement

Financial support for AY provided by the UK Engineering and Physical Sciences Research Council (Grant GR/594469/01) is gratefully acknowledged.

References:

[1] A.L. Yerokhin, X. Nie, A. Leyland, A. Matthews and S.J. Dowey, Surf. and Coat. Technol. **122**, (1999) 73–93

[2] A.L. Yerokhin, X. Nie, A. Leyland and A. Matthews, Surf. and Coat. Technol. **130**, (2000) 195–206

[3] T.H. Teh, A. Berkani, S. Mato, P. Skeldon, G.E. Thompson, H. Habazaki and K. Shimizu, Corros. Sci. **45** (2003) 2757–2768

[4] Y. Han, S.-H. Hong and K.W. Xu, Surf. and Coat. Technol. **154** (2002) 314-318

[5] ASM Metals Handbook, *Surface Engineering*, vol. **5**, (1994) pp. 1765–1782

[6] F. Badawai and P. Villain, J. Appl. Cryst. **36** (2003) 869–879

[7] G.J. Exarhos and N.J. Hess, Thin Solid Films **220** (1992) 254–260

[8] S.G. Croll, J. Appl. Polm. Sci. **23** (1979) 847

[9] L.C. Archibald, Electrochimica Acta **22** (1977) 657–659.

[10] J. Kim, S. Pyun, M. Seo, Electrochimica Acta **48** (2003) 1123–1130

[11] Y.-P. Lu, M.-S. Li, S.-T. Li, Z.-G. Wang, R.-F. Zhu, Biomaterials 25 (2004) 4393-4403

[12] J.C. Nelson, R.A. Oriani, Corros. Sci. **34** (1993) 307–326

[13] C.R. Ottermann, K. Bange, Thin Solid Films, **286** (1996) 32–34

[14] P. Huang, K. Xu, B. He, Y. Han, Mater. Sci. Forum **490-491** (2005) 552–557

[15] P. Huang, F. Wang, K. Xu, Y. Han, Surf. and Coat. Technol. **201** (2007) 5168–5171

[16] R.H.U. Khan, A.L. Yerokhin, T. Pilkington, A. Leyland and A. Matthews, Surf. and Coat. Technol. **200** (2005) 1580–1586

[17] X.-Z. Ding and X.-H. Liu, J. Mater. Sci. Lett. **15**, (1996) 1789-1791

[18] R.A. Spurr and H. Myers, *Anal. Chem.* **29** (1957) 760

[19] B.D. Cullity and S.R. Stock, *Elements of X-ray diffraction*, **3**rd ed. (2001), pp. 170

[20] I. Kraus, N. Ganev, G. Gosmanova, H.-D. Tietz, L. Pfeiffer, S. Bohm, Mater. Sci. Eng., **A199** (1995) L15–L17

[21] Bruker Advanced X-ray Solutions, Diffrac^plus Stress, Bruker AXS GmbH, Karlsruhe, Germany, 1998–1999

[22] A.H.C. Chan, J.F. Porter, J.P. Barford and C.K. Chan, J. Mater. Res. Vol. **17**, No. 7 (2002) 1758-1765

[23] H. Ishizawa, M. Ogino, J. Biomed. Mater. Res. **29** (1994) 65–72

[24] B.S. Ng, I. Annergren, A.M. Soutar, K. A. Khor, A.E.W. Jarfors, Biomaterials **26** (2006) 1087–1095

[25] A. Michelmore, W. Gong, P. Jenkins and J. Ralston, Phys. Chem. Chem. Phys., **2** (2000) 2985–2992

[26] A.I. Bortun, L. Bortun and A. Clearfield, J. Mater. Res. Vol. **11**, 10 (1996) 2490–2498

[27] L. Muller and F.A. Muller, Acta Biomaterialia, **2** (2006) 181–189

[28] O. Zywitzki, T. Modes, H. Sahm, P. Frach, K. Goedicke and D. Gloß, Surf. and Coat.Technol. **180–181** (2004) 538-543

[29] http://www.matweb.com, Materials property data, online Material Data Sheet, titania.

[30] L.O. Snizhko, A.L. Yerokhin, A. Pilkington, N.L. Gurevina, D.O. Misnyankin, A. Leyland, A. Matthews, Electrochimica Acta, **49** (2004) 2085-2095

[31] L.O. Snizhko, A.L. Yerokhin, A. Pilkington, N.L. Gurevina, D.O. Misnyankin, A. Leyland, A. Matthews, Electrochimica Acta, **50** (2005) 5458-5464

[33] E. Matykina, G. Doucet, F. Monfort, A. Berkani, P. Skeldon, G.E. Thompson, Electrochimica Acta, **51** (2006) 4709-4715

[34] E. Matykina, R. Arrabal, P. Skeldon, G.E. Thompson, H. Habazaki, Thin Solid Films, (2007) in press. doi:10.1016/j.tsf.2007.08.104

[35] Y. Guangliang, L. Xianyi, B. Yizhen, C. Haifeng, J. Zengsun, J. Alloys and Compounds, 345 (2002) 196–200

[36] P.S. Gordienko, S.V. Gnedenkov, Microarc Oxidation of Titanium and Its Alloys, Dalnauka, Vladivostok, (1997) 185 p.

Figure Captions

Fig. 1. Characteristic voltage and current waveforms employed in pulsed unipolar PEO of cp-Ti at a constant mean average current density i = 10 A/dm^2 (f = 100 Hz).

Fig. 2. Typical X-ray diffraction pattern of the oxide ceramic coating formed on cp-Ti by pulsed unipolar PEO.

Fig. 3. Characteristic peaks of (a) (215) anatase and (b) (222) rutile planes in XRD patterns of pulsed unipolar PEO titania coatings taken at different ψ angles.

Fig. 4. SEM micrographs showing (a) characteristic surface morphology; (b) nanostructured globular features on the surface of PEO coatings formed on cp-Ti in Na_3PO_4 electrolyte at f = 10 kHz and δ = 0.8; (c) EDX spectrum corresponding to (a). Note that oxygen is not detectable with the EDX attachment used.

Fig. 5. Relative rutile in PEO coatings on Ti produced at various current frequencies and duty cycles.

Fig. 6. Typical FT-IR spectrum of PEO titania coatings showing the presence of polyphosphates, i.e. PO_2^-, PO_3^{2-} and PO_4^{3-} at frequencies/cm^{-1} 1250-1290, 1160-1170 and 840-870 respectively.

Fig. 7. STM cross-sectional micrograph of PEO titania coating (a) and corresponding maps of the coating hardness (b) and Young's modulus (c).

Fig. 8. Effect of pulse frequency and duty cycle on (a) direct and (b) shear stresses in the anatase phase constituent of PEO coatings produced using pulsed unipolar current.

Fig. 9. Effect of pulse frequency and duty cycle on (a) direct and (b) shear stresses in the rutile phase constituent of PEO coatings produced using pulsed unipolar current.

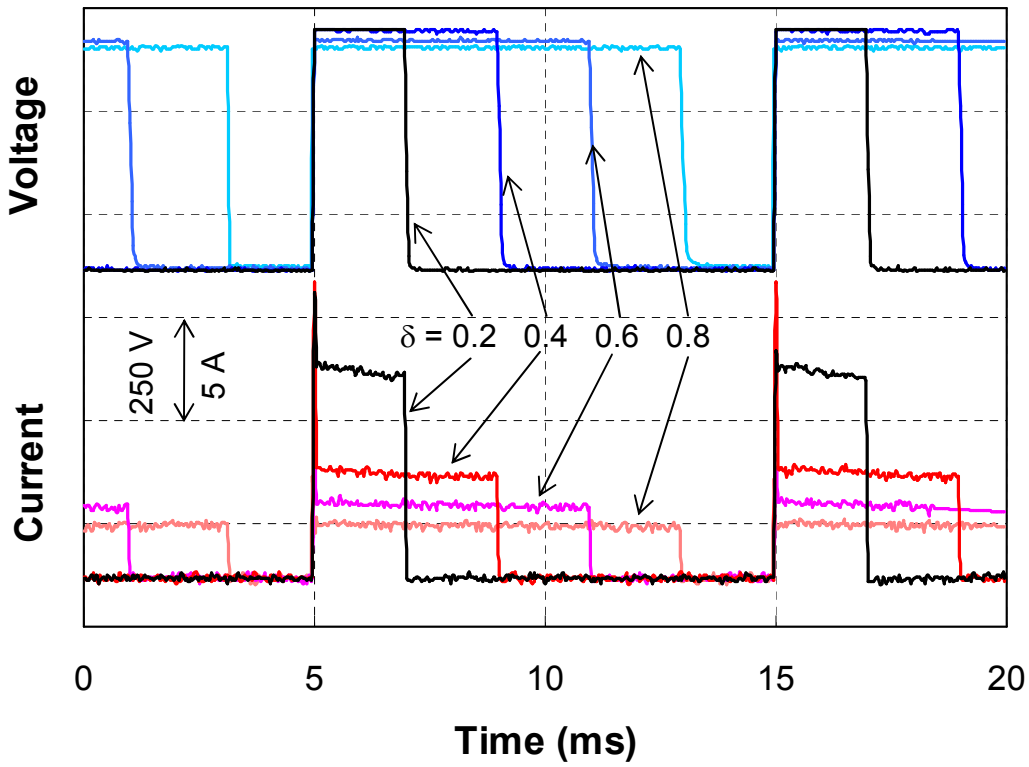

Fig. 1. Characteristic voltage and current waveforms employed in pulsed unipolar PEO of cp-Ti at a constant mean average current density i = 10 A/dm^2 (f = 100 Hz).

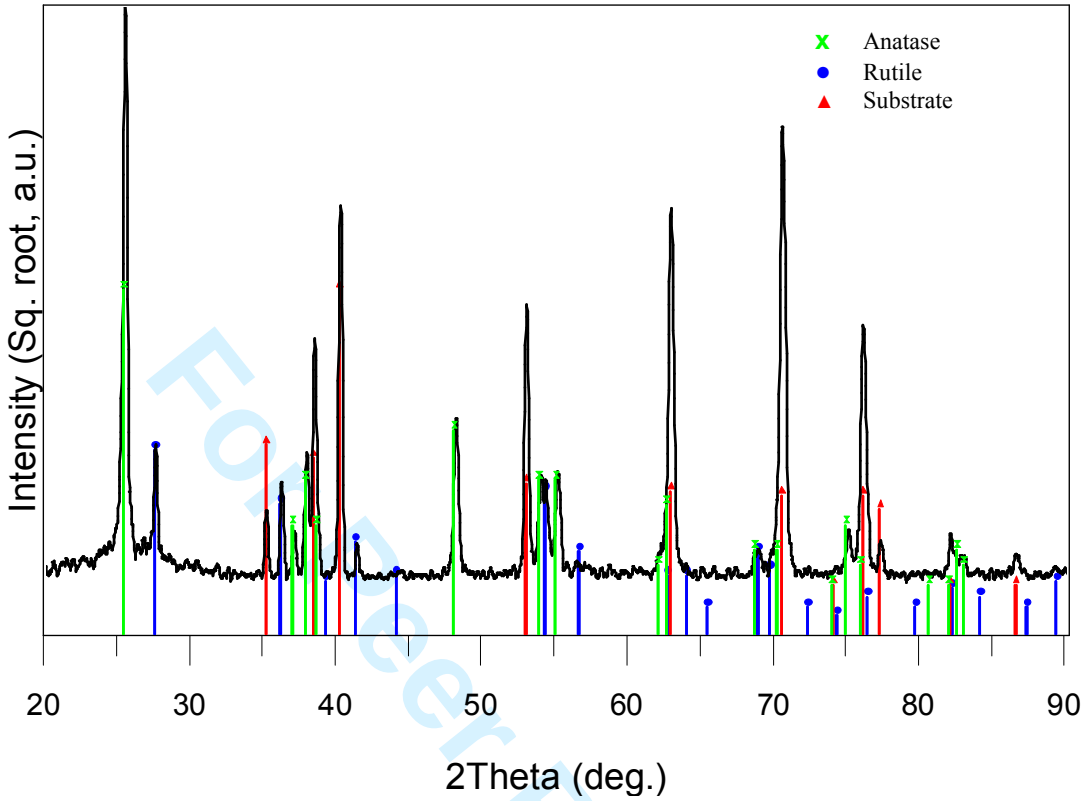

Fig. 2. Typical X-ray diffraction pattern of the oxide ceramic coating formed on cp-Ti by pulsed unipolar PEO.

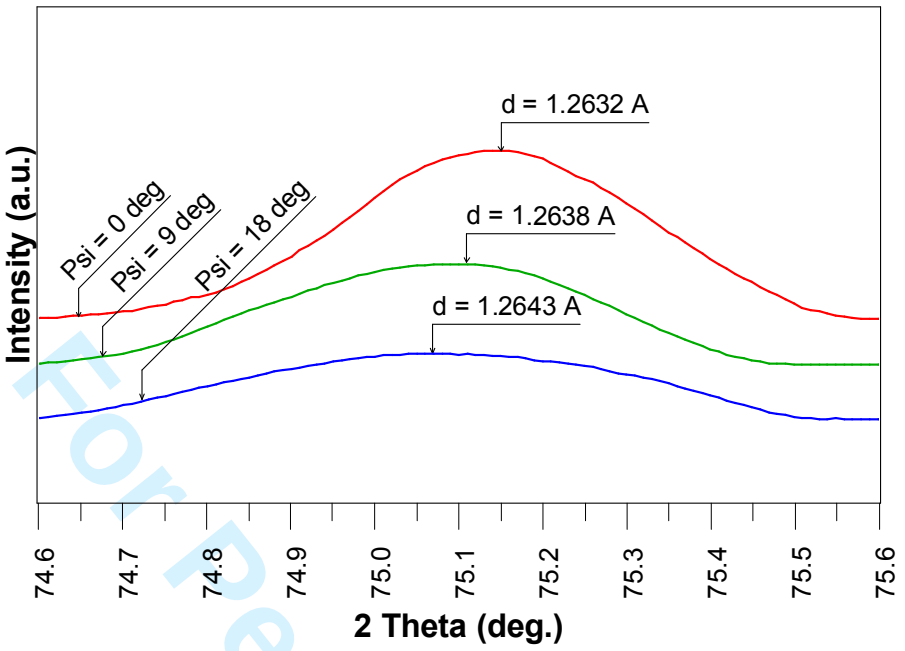

(a)

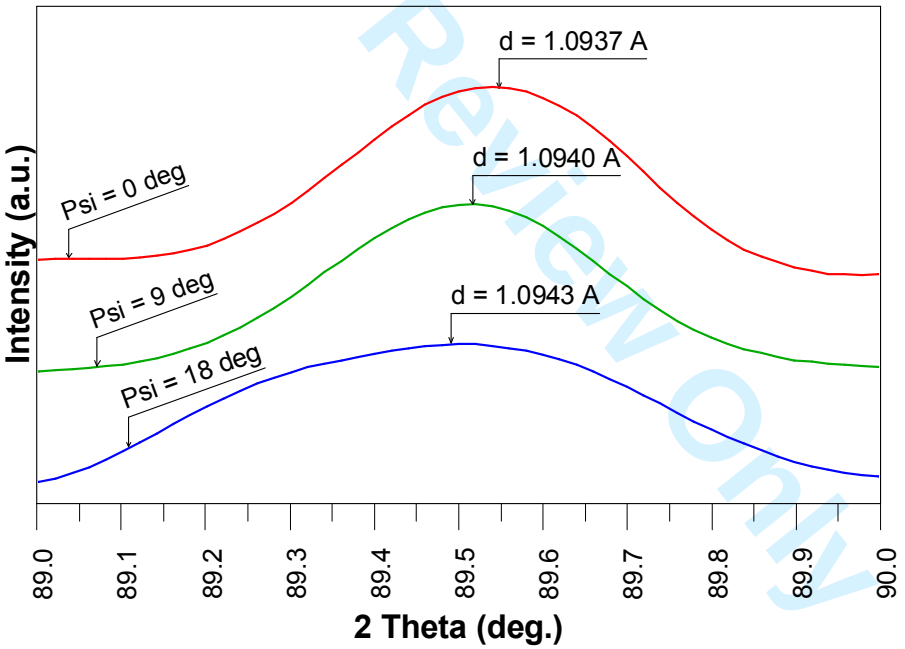

(b)

Fig. 3. Characteristic peaks of (a) (215) anatase and (b) (222) rutile planes in XRD patterns of pulsed unipolar PEO titania coatings taken at different ψ angles.

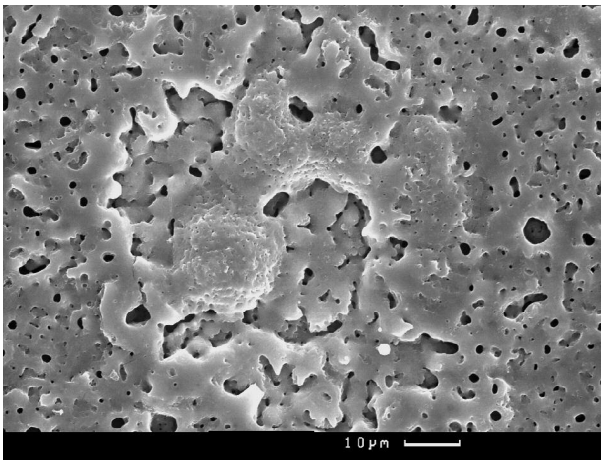

(a)

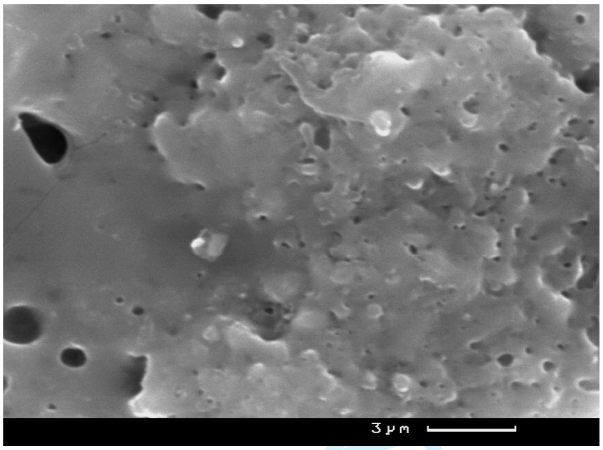

(b)

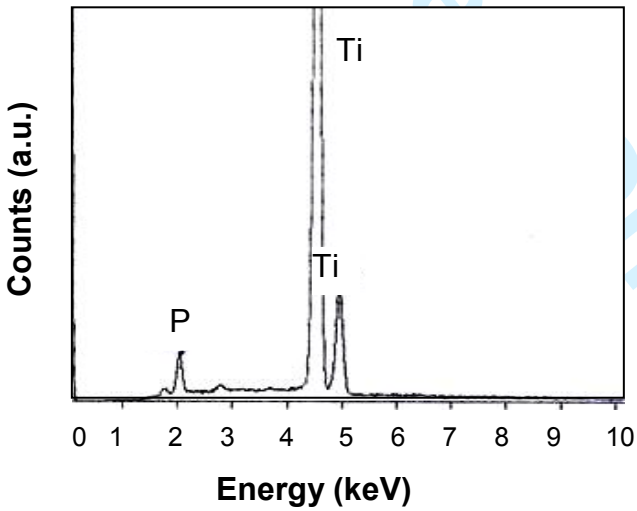

(c)

Fig. 4. SEM micrographs showing (a) characteristic surface morphology; (b) nanostructured nodular features on the surface of PEO coatings formed on cp-Ti in Na_3PO_4 electrolyte at f = 10 kHz and δ = 0.8; (c) EDX spectrum corresponding to (a). Note that oxygen is not detectable with the EDX attachment used.

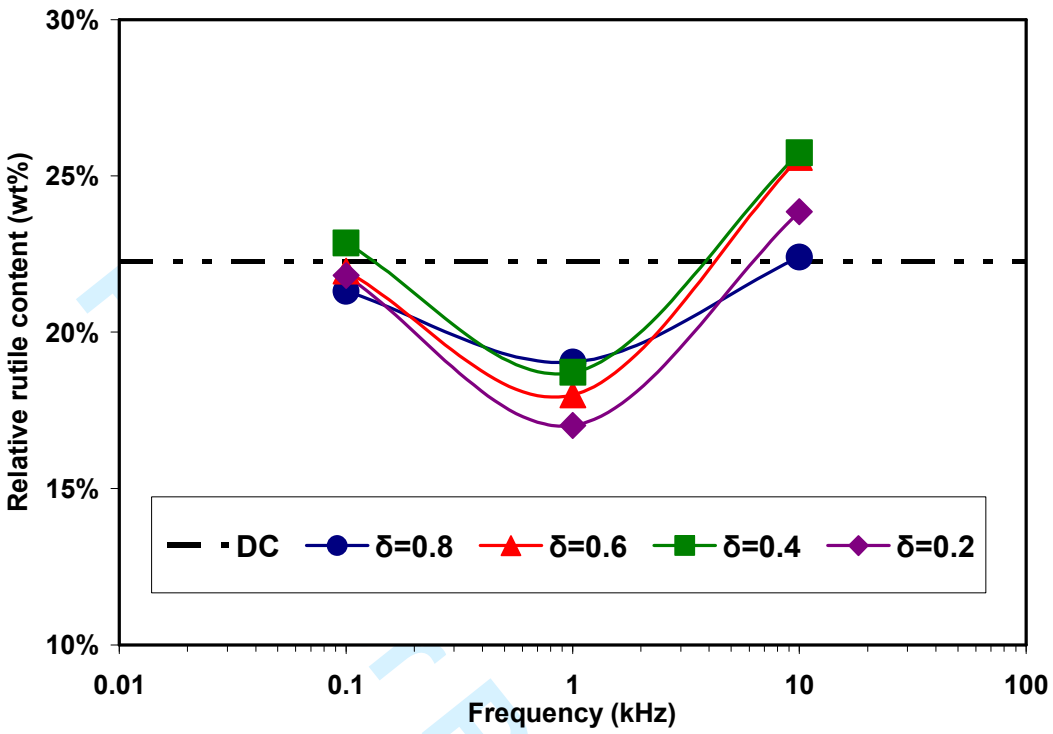

Fig. 5. Relative rutile in PEO coatings on Ti produced at various current frequencies and duty cycles.

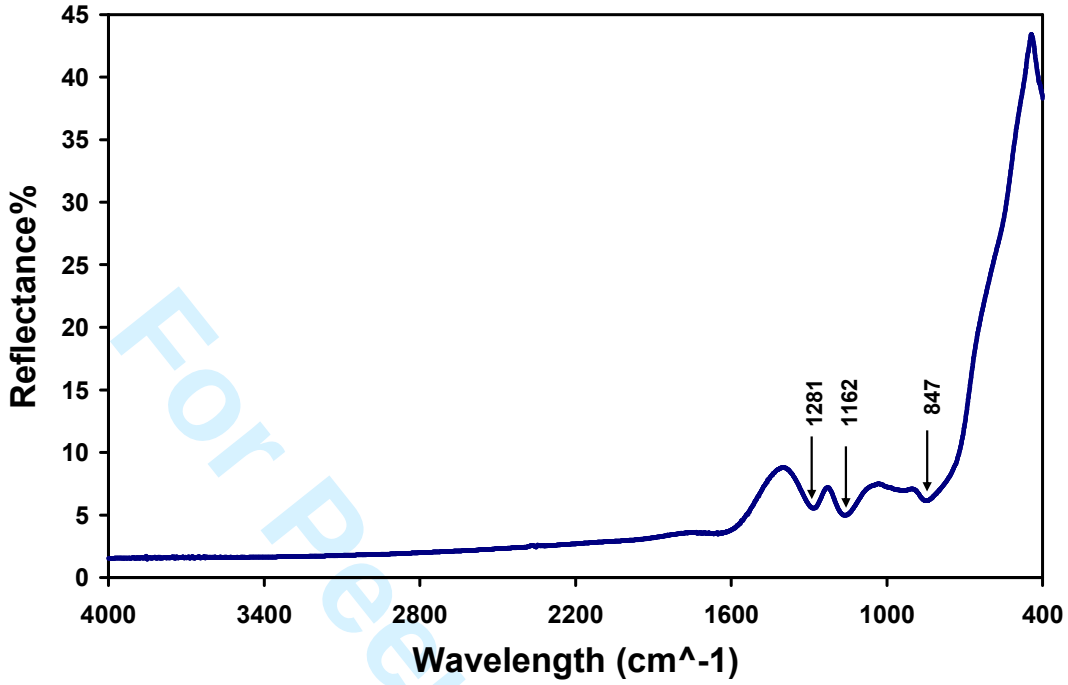

Fig. 6. Typical FT-IR spectrum showing the presence of PO_2^-, PO_3^{2-} and PO_4^{3-} polyphosphates at frequencies/cm^{-1} 1250-1290, 1160-1170 and 840-870 respectively in PEO titania coatings.

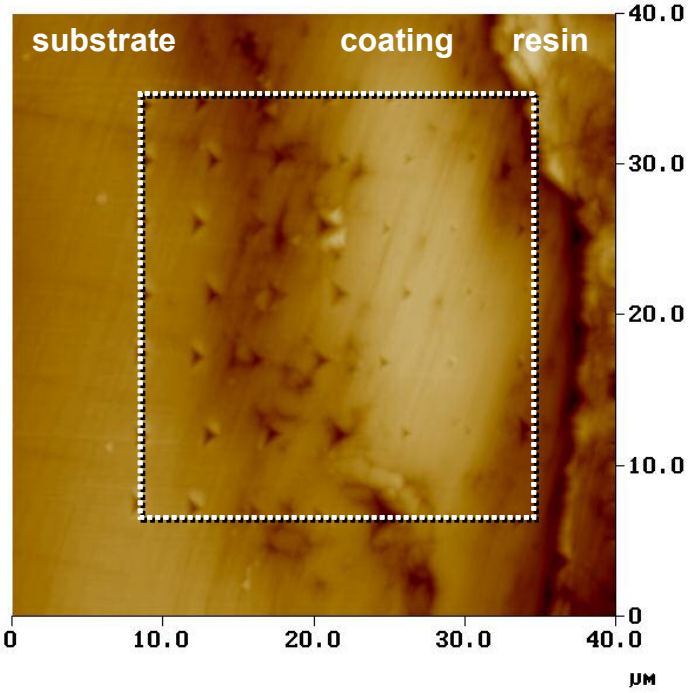

(a)

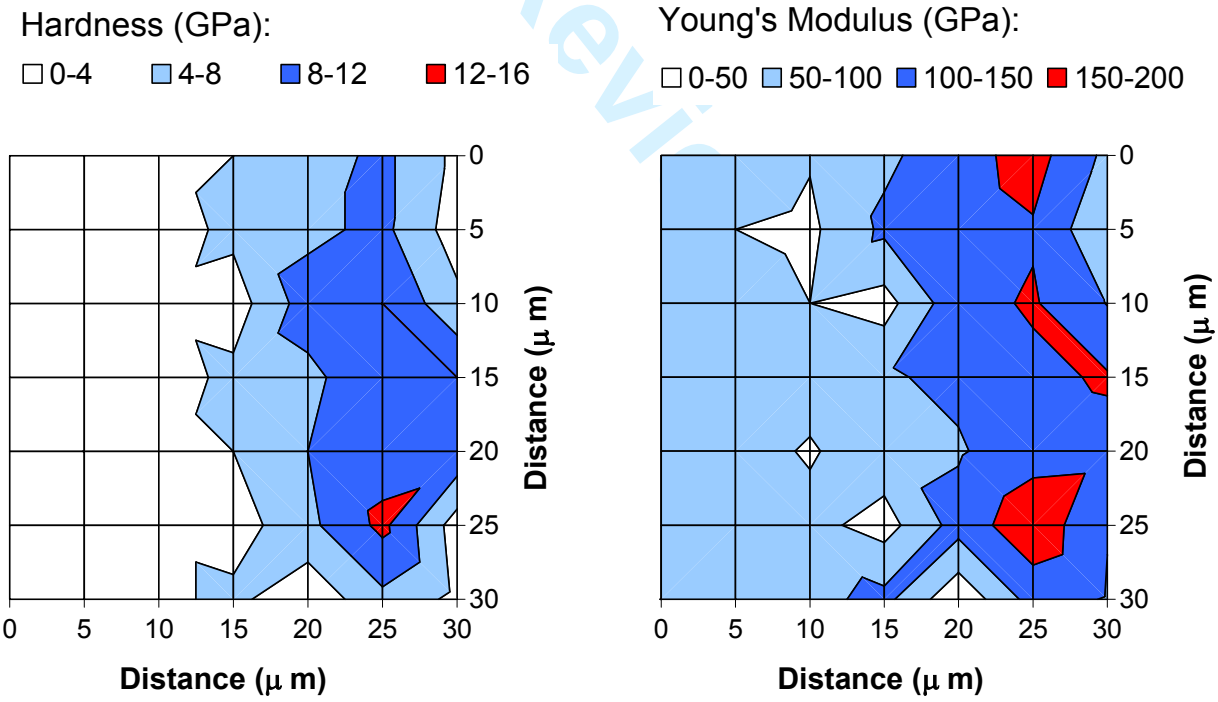

(b) (c)

Fig. 7. STM cross-sectional micrograph of PEO titania coating (a) and corresponding maps of the coating hardness (b) and Young's modulus (c).

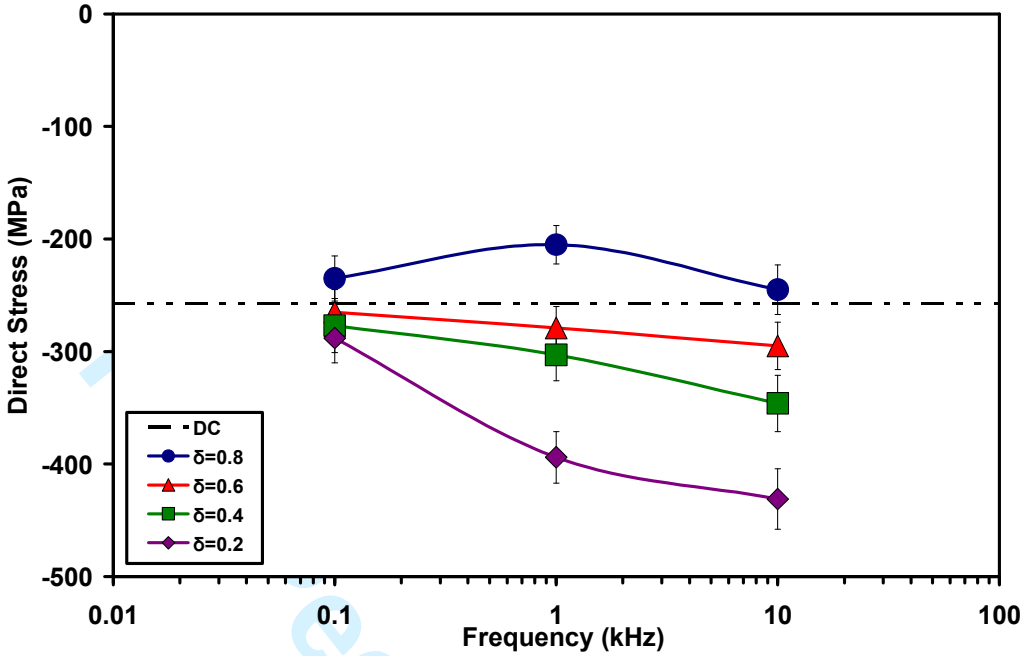

(a)

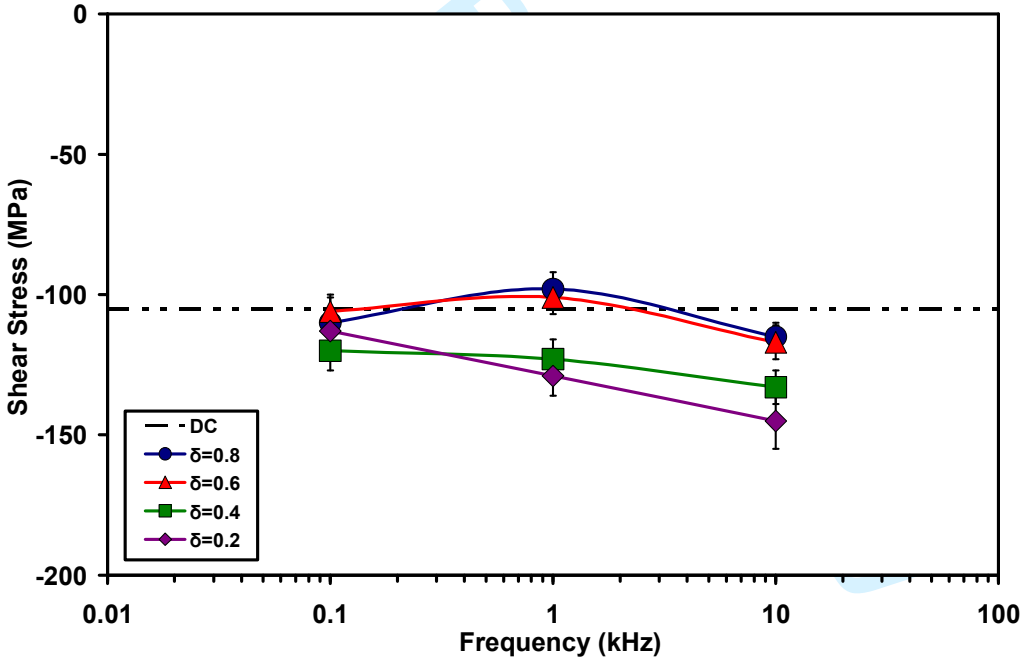

(b)

Fig. 8. Effect of pulse frequency and duty cycle on (a) direct and (b) shear stresses in the anatase phase constituent of PEO coatings produced using pulsed unipolar current.

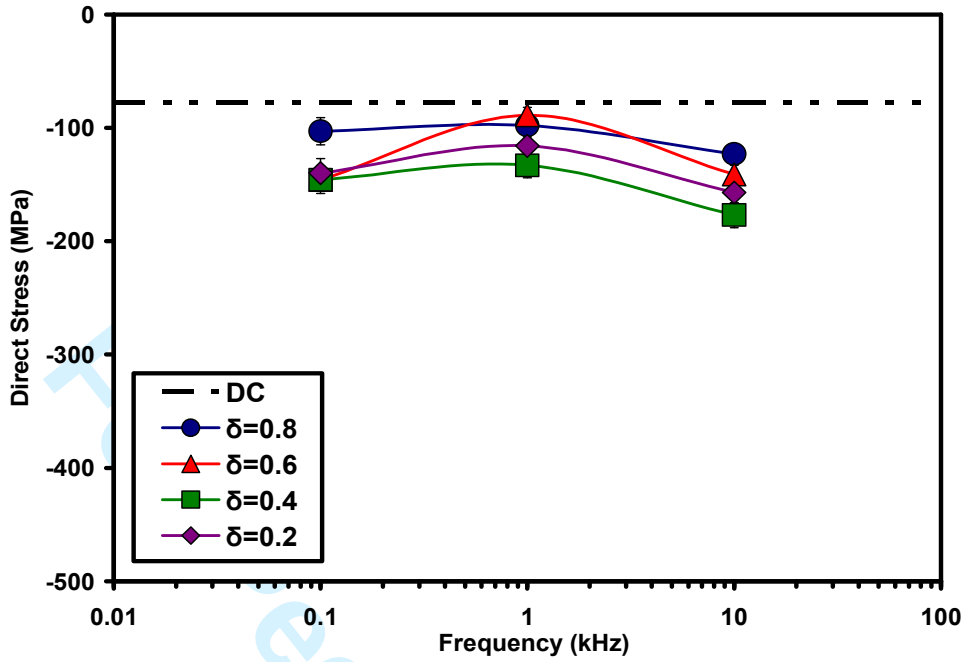

(a)

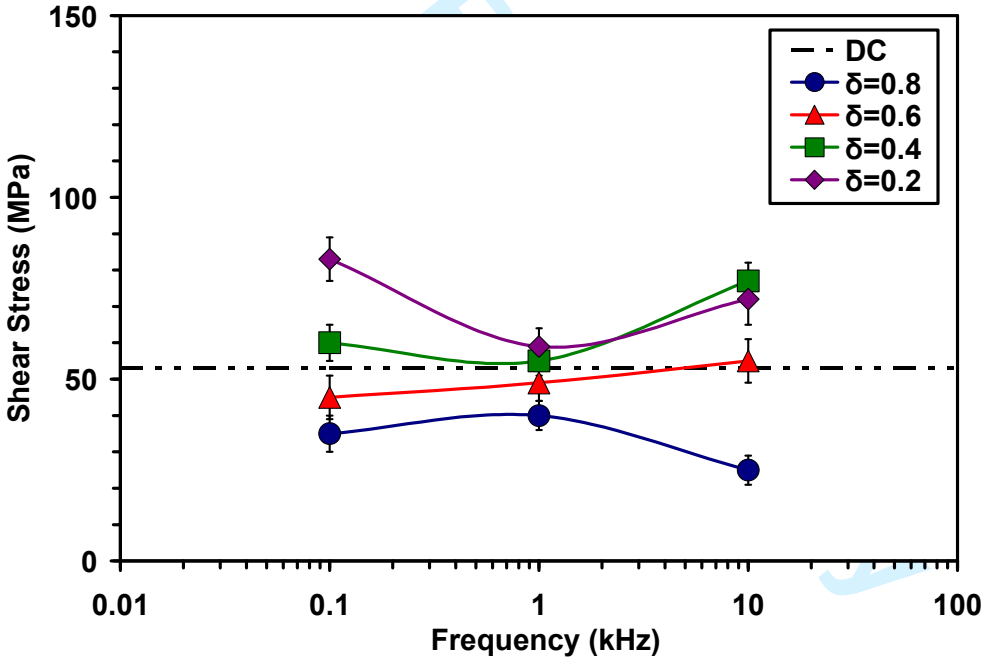

(b)

Fig. 9. Effect of pulse frequency and duty cycle on (a) direct and (b) shear stresses in the rutile phase constituent of PEO coatings produced using pulsed unipolar current.